American Mineralogist, Volume 84, pages 1595–1603, 1999

The $MgTiO_3$-$FeTiO_3$ join at high pressure and temperature

JENNIFER A. LINTON,[1,*] YINGWEI FEI,[2] AND ALEXANDRA NAVROTSKY[3]

[1]Department of Geosciences and Center for High Pressure Research, Princeton University, Princeton, New Jersey 80544, U.S.A.
[2]Geophysical Laboratory and Center for High Pressure Research, Carnegie Institution of Washington, 5251 Broad Branch Road, N.W., Washington, D.C. 20015, U.S.A.
[3]Thermochemistry Facility and Center for High Pressure Research, Department of Chemical Engineering and Materials Science, University of California at Davis, Davis, California 95616, U.S.A.

ABSTRACT

The phase relations at high pressure and high temperature for the $FeTiO_3$-$MgTiO_3$ join were determined using several different experimental methods. Through a series of multi-anvil experiments, a phase boundary with a negative slope was observed between $MgTiO_3$ I (ilmenite structure) and a high pressure phase with the $MgTiO_3$ II (lithium niobate structure) after quenching. The enthalpy of transformation of $MgTiO_3$ I to $MgTiO_3$ II was determined through transposed-temperature-drop calorimetry to be 28.78 ± 1.45 kJ/mol. The enthalpy of transformation from ilmenite to lithium niobate structure was also determined for three intermediate compositions on the $FeTiO_3$-$MgTiO_3$ join, $Fe_{0.2}Mg_{0.8}TiO_3$, $Fe_{0.5}Mg_{0.5}TiO_3$ and $Fe_{0.8}Mg_{0.2}TiO_3$, and confirmed for $FeTiO_3$, and was found to be a linear function of composition. These experiments represent one of the first successful calorimetric measurements on small samples (1 to 3 mg) synthesized at high pressures (15 to 21 GPa). X-ray analysis during compression of $Fe_{0.5}Mg_{0.5}TiO_3$ II in a diamond cell confirmed a room temperature transition at 28 GPa to $Fe_{0.5}Mg_{0.5}TiO_3$ III (a $GdFeO_3$-type perovskite structure), similar to the transitions previously observed in $FeTiO_3$ and $MnTiO_3$. The $Fe_{0.5}Mg_{0.5}TiO_3$ sample was heated to 802 °C at 21 GPa, and it was observed that the stable high temperature, high pressure phase is perovskite, $Fe_{0.5}Mg_{0.5}TiO_3$ III. The above data combined confirm the stability of a continuous perovskite solid solution at high pressure and temperature for the $FeTiO_3$-$MgTiO_3$ join.

INTRODUCTION

Under ambient conditions, both $FeTiO_3$ and $MgTiO_3$ are stable in the ilmenite structure ($R\bar{3}$), and complete solid solution occurs between them (e.g., Wood et al. 1991). Syono et al. (1980) described a phase transition at high pressures in $FeTiO_3$ from the ilmenite structure ($FeTiO_3$ I) to a hexagonal structure seen in multi-anvil quench experiments and later determined to be the lithium niobate structure ($FeTiO_3$ II) (Leinenweber et al. 1995; Ko and Prewitt 1988). At 16 GPa $FeTiO_3$ in this lithium niobate structure transforms to an orthorhombic perovskite polymorph ($FeTiO_3$ III) (Leinenweber et al. 1991). During quenching this perovskite ($FeTiO_3$ III) reverted to the lithium niobate structure (Leinenweber et al. 1991). Thermodynamic calculations, based on the observed *P-T* diagram and on the measured enthalpy of II-to-I transition, indicated the stable $FeTiO_3$ phase at high pressure has the perovskite structure while the lithium niobate polymorph is a metastable quench phase (Mehta et al. 1994).

A new high-pressure $MgTiO_3$ phase with the lithium niobate structure ($R3c$) ($MgTiO_3$ II) was recovered after synthesis at 21 GPa and 1200 °C, and phases with the lithium niobate structure were also synthesized for intermediate compositions between $FeTiO_3$ and $MgTiO_3$ (Linton et al. 1997). These magnesium-iron titanates with lithium niobate structures may be metastable quench phases from perovskites. This study shows through calorimetry and X-ray diffraction during compression of $MgTiO_3$-$FeTiO_3$ with the lithium niobate structure in a diamond anvil cell (DAC) that these compounds are stable in perovskite-type structures at high pressure. This is the first example of a complete solid solution between iron and magnesium in the perovskite structure.

EXPERIMENTAL METHODS

Synthesis

The geikielite ($MgTiO_3$ I) starting material was synthesized from stoichiometric quantities of MgO and TiO_2 ground together under ethanol for one hour. Both MgO and TiO_2 were dried prior to weighing in Pt crucibles at 1400 and 1150 °C, respectively, for ~24 hours. The mixture was first heated at 1200 °C for 48 hours and then reground and heated for 24 hours at 1450 °C. The temperature was reduced to 800 °C and the sample removed and cooled in a desiccator. X-ray diffraction patterns of the product showed only geikielite peaks.

$MgTiO_3$-$FeTiO_3$ ilmenite solid solutions were synthesized from mixtures of predried Fe_2O_3 and TiO_2 plus $MgTiO_3$. The mixture was ground in an agate mortar for 1 hour, then heated

*Current address: Basic Energy Sciences Synchrotron Radiation Center and Materials Science Division, Argonne National Laboratory, 9700 S. Cass Avenue, Argonne, Illinois 60439 U.S.A. E-mail: linton@anl.gov

in a platinum crucible at 1200 °C. The oxygen fugacity was controlled at $10^{-10.5}$ atm by a flow of CO and CO_2. To limit iron loss to the platinum, two lots for each composition were sequentially reacted in the same crucible and the first batch was thrown away. The purity of the products was confirmed by XRD, microprobe and Mössbauer analyses.

Samples of $MgTiO_3$, $Fe_{0.2}Mg_{0.8}TiO_3$, $Fe_{0.5}Mg_{0.5}TiO_3$, $Fe_{0.8}Mg_{0.2}TiO_3$, and $FeTiO_3$ in the lithium niobate structure were synthesized from ilmenites of the same composition in a multi-anvil press at the Geophysical Laboratory at 21 GPa and 1300 °C, 19 GPa and 1300 °C, 20 GPa and 1300 °C, 15 GPa and 1300 °C, and 15 GPa and 1300 °C, respectively. Experiment durations ranged from 3 to 24 hours. Each entire sample was removed from its capsule onto a quartz low-background plate and X-rayed. A small quantity of sample was reserved for microprobe analysis (no cation inhomogeneities were found in fully reacted material).

Calorimetry

Transposed temperature drop calorimetry was performed using a miniaturized "ultra-sensitive" Calvet-type calorimeter optimized for use with very small samples (Topor and Navrotsky 1992; Navrotsky 1997). The 2 to 2.5 mg pressed pellets of $MgTiO_3$ I, $FeTiO_3$ I, $MgTiO_3$ II, and $FeTiO_3$ II were dropped from room temperature (22 °C) to a calorimeter temperature of 801 °C. Fe bearing samples were dropped under a flow of argon, which had been purified by a commercial oxygen getter down to 10 ppb O_2. Phase II samples were dropped, calorimetric signal was measured for forty minutes, and the samples were rapidly withdrawn from the calorimeter to room temperature. This was done to avoid any slow further transformation of the samples which might be undetected in the calorimetric signal. The samples were then repelletized, weighed, and dropped again. Occasionally, when the sample was broken into too many small pieces on the first drop, it was impossible to collect enough sample (>0.5 mg) to form a pellet for a second drop.

High-pressure phase equilibrium

The high pressure and temperature experiments were conducted in a Walker-type multi-anvil press at the Geophysical Laboratory of the Carnegie Institution of Washington. Two types of assemblies were used; for 5 to 9 GPa experiments (synthesis of $FeTiO_3$ II), we used a 18 mm edge length cast MgO octahedron with a graphite heater and gold or iron capsules. For 10–15 GPa experiments, a MgO octahedral pressure medium with 10 mm edge lengths was used, with 0.5–1 mm in diameter by 1–2 mm in length gold capsules separated by a MgO sleeve from a Re foil heater with a thermal gradient of less than 50 °C over the length of the capsule. Temperature was measured with W5%Re-W26%Re (Type C) thermocouples. Eight tungsten carbide cubes with a corner truncation of 11 mm for lower pressures or 5 mm for higher pressures applied a compressive force on the octahedra. Samples were fully pressurized at a rate of 2–5 GPa/hour then heated at 20 to 80 °C/min. At the end of the run, samples were thermally quenched by cutting off power to the furnace, then slowly depressurized. The pressure calibration at high temperature (e.g., 1200 °C) was established by determining transitions for well-known reactions in Bi, SiO_2, Fe_2SiO_4, Mg_2SiO_4, and $CaGeO_3$ (Bertka and Fei 1996).

After the runs, samples were embedded in epoxy and polished. Major element mineral analyzes were acquired using a JEOL JXM 8900 microprobe. The acceleration voltage was 15 kV and the beam current was 20 nA. The locations for analysis and imaging were obtained in a backscattered electron mode. X-ray patterns were obtained on a Scintag XDS-2000 powder diffractometer with a solid-state detector equipped with a Ge crystal using Cu*K*α radiation.

Diamond-anvil cell experiments

Polychromatic (white) wiggler synchrotron x-radiation from X-ray beam line X17c at the National Synchrotron Light Source at Brookhaven National Laboratory was used for energy dispersive X-ray diffraction experiments. Samples were contained by a rhenium gasket between two gem-quality diamonds which applied pressure on the samples. The cells were heated by a Mo-wire resistance heater situated inside the cylinder of the cell around the diamond anvils and by a separate platinum wire resistance heater surrounding the cylinder segment of the cell. This combination of heaters allowed the whole sample to be heated uniformly up to ~800–900 °C; for details see Fei (1996). Pressure was determined by including small pieces of gold foil and referring to the *P-V-T* equation of state of gold by Anderson et al. (1989). Because no pressure medium was used and the pressure gradient across the cell could be as great as 10 GPa, spectra were taken including both gold and sample peaks. Temperature was measured with a Pt-Pt13%Rh thermocouple with its contact on the gasket near the sample.

Raman spectra

Raman spectra of $MgTiO_3$ samples were excited using the 514 nm line from an Ar^+ ion argon laser, and recorded with an EG&G Model 4000 CCD with acquisition times up to 20 minutes. Spectra were collected from polished samples embedded in epoxy using a petrographic microscope attached to the micro-Raman system (625× magnification) to determine whether the samples had transformed from $MgTiO_3$ I to $MgTiO_3$ II in phase equilibrium studies.

RESULTS

Calorimetry

Transposed temperature drop measurements were made for $FeTiO_3$-$MgTiO_3$ solid solutions in both the ilmenite and lithium niobate structures. The heat effect for each ilmenite listed in Table 1 is simply the heat content of the sample, because ilmenite is stable at the calorimeter temperature of 801 °C. Our values are ~4% lower than the heat contents of $MgTiO_3$ and

TABLE 1. Heat content of $FeTiO_3$-$MgTiO_3$ I (ilmenite structure)

Formula	Heat content* (kJ/mol)
$MgTiO_3$	88.58 ± 2.03(7)
$Fe_{0.2}Mg_{0.8}TiO_3$	89.63 ± 1.06(4)
$Fe_{0.5}Mg_{0.5}TiO_3$	91.22 ± 0.63(6)
$Fe_{0.8}Mg_{0.2}TiO_3$	92.06 ± 1.11(6)
$FeTiO_3$	92.56 ± 0.50(6)

Notes: Error represents two standard deviations of the mean. The values in parentheses is number of experiments for each composition.
* $(H_{295K} - H_{1074K})$.

$FeTiO_3$ of Robie and Hemingway (1995). This difference appears to be systematic and is possibly due to a problem in our calibration, but it should not significantly affect our results for the enthalpy of transition. The heat effect for the lithium niobates contains the heat content and the heat of transformation from lithium niobate to ilmenite structure. The complete transformation with no amorphization of the sample was attained by rapidly removing samples from the calorimeter after forty minutes at 801 °C and confirmed through optical examination and X-ray diffraction of end-member composition samples. The agreement of the second transposed temperature drop measurement with the heat content of an ilmenite of the same composition is consistent with complete transformation of the lithium niobate to ilmenite structures (Table 2). To calculate the enthalpy of transition (Table 3, Fig. 1) for each composition, the difference was calculated between the transposed temperature drop measurement of the lithium niobate and the average heat content for ilmenite (although the difference between the first and second drop could also be used to give results that agree within error). There is some scatter, but a linear trend between the two end-members is evident. The present enthalpy of transition (I → II) for pure $FeTiO_3$, –14.52 (2.16) kJ/mol, is within error of the –13.5(1.2) kJ/mol obtained by Mehta et al. (1994), who used much larger pellets (10–30 mg).

TABLE 2. Transposed-temperature-drop calorimetric measurements on $FeTiO_3$-$MgTiO_3$ II (lithium niobate structure)

	First drop		Second drop	
	Mass (mg)	Heat content* + heat of transition (kJ/mol)	Mass (mg)	Heat content* (kJ/mol)
$MgTiO_3$	1.098	60.52	0.992	87.27
	1.719	59.06	1.536	88.73
$Fe_{0.2}Mg_{0.8}TiO_3$	0.862	69.00		
$Fe_{0.5}Mg_{0.5}TiO_3$	1.756	69.78	1.499	92.23
	1.375	66.90	1.267	88.11
	0.889	71.11		
$Fe_{0.8}Mg_{0.2}TiO_3$	1.239	78.88	0.665	89.92
	0.996	72.45	0.712	86.41
	1.458	79.73	2.137†	91.50
	0.958	71.03	2.137†	91.50
$FeTiO_3$	2.481	80.09	2.345†	91.62
	1.419	77.56	2.345†	91.62
	1.445	76.44	1.315	89.09

* $(H_{295K} - H_{1074K})$.
† Pellet made from combination of two reacted $MgTiO_3$ pellets.

TABLE 3. Reaction enthalpy for I to II transition

	ΔH of transformation (kJ/mol)	No. of expts.
$MgTiO_3$	–28.78 ± 1.45	2
$Fe_{0.2}Mg_{0.8}TiO_3$	–20.63	1
$Fe_{0.5}Mg_{0.5}TiO_3$	–21.96 ± 2.15	3
$Fe_{0.8}Mg_{0.2}TiO_3$	–16.54 ± 4.42	4
$FeTiO_3$	–14.52 ± 2.16	3

Notes: Calculated using the average difference between the lithium niobate heat content and the average ilmenite heat content of the same composition. Errors are two standard deviations from the mean.

Phase stability

Although the high-pressure experiments are not reversals, they provide an upper limit for the phase boundary (Fig. 2). The reactions occur quickly (some experiments forming the high pressure phase were under 0.5 h). The boundary of the transition, calculated by a least squares fit to all the data, is P(GPa) = –0.008(2)T(K) + 33(4). The slope of this boundary is very similar to that found for pure $FeTiO_3$: P(GPa) = –0.01(3)T(K) + 25(4) (Mehta et al. 1994; Syono et al. 1980). The $FeTiO_3$ I-II transition occurs 8–10 GPa lower than that of $MgTiO_3$ at comparable temperatures.

Raman spectra

The Raman spectrum of $MgTiO_3$ II (Fig. 3) is similar to the spectrum of the lithium niobate polymorph of $MnTiO_3$ (Ko et al. 1989), and also that of its ilmenite polymorph, but the $MgTiO_3$ II spectrum exhibits more bands due to its lower symmetry. The higher frequency bands also occur at lower energies for the lithium niobate form, which can be associated with higher entropy for the lithium niobate structure (Ko et al. 1989; Kieffer 1985).

Diamond anvil-cell experiments

$MgTiO_3$ with the lithium niobate structure recovered from multi-anvil experiments was compressed in a DAC without a pressure medium. During compression of $Mg_{0.5}Fe_{0.5}TiO_3$ II, a phase transformation was observed at room temperature and 30 GPa. Based on comparison to the X-ray peaks of the new phase of $FeTiO_3$ III (Leinenweber et al. 1991) and $MnTiO_3$ III (Ross et al. 1989), the new phase was indexed as an orthorhombic perovskite ($GdFeO_3$-type, space group *Pbnm*). The

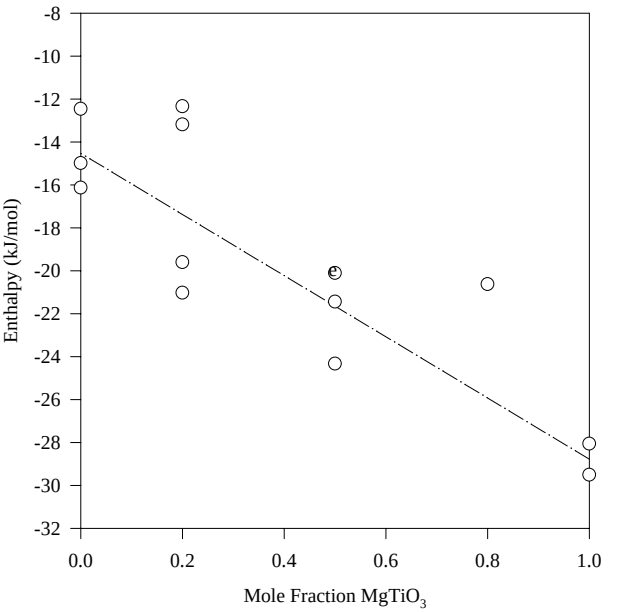

FIGURE 1. Enthalpy of the II to I transitions for $FeTiO_3$-$MgTiO_3$ for individual calorimetric experiments from five compositions. Dash-dotted line connects the end-members.

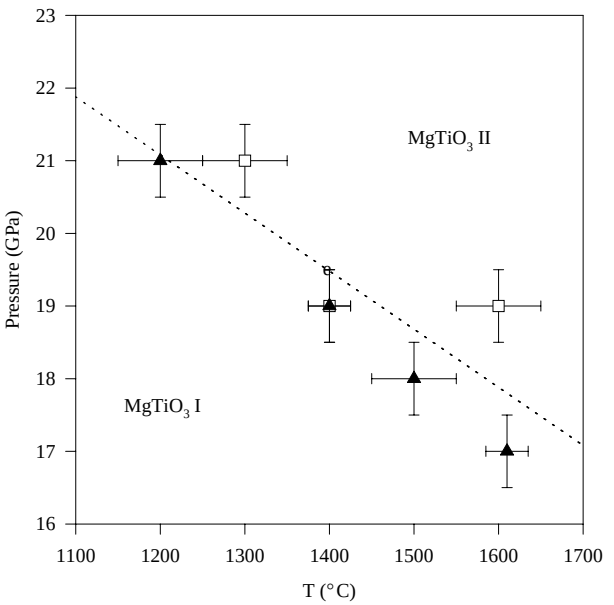

FIGURE 2. Phase diagram for $MgTiO_3$ I → $MgTiO_3$ II samples recovered after quench. Filled triangles = $MgTiO_3$ I; unfilled squares = formation of $MgTiO_3$ II; the dotted line is our calculated phase boundary: P(GPa) = –0.008(2)T(K) + 33(4).

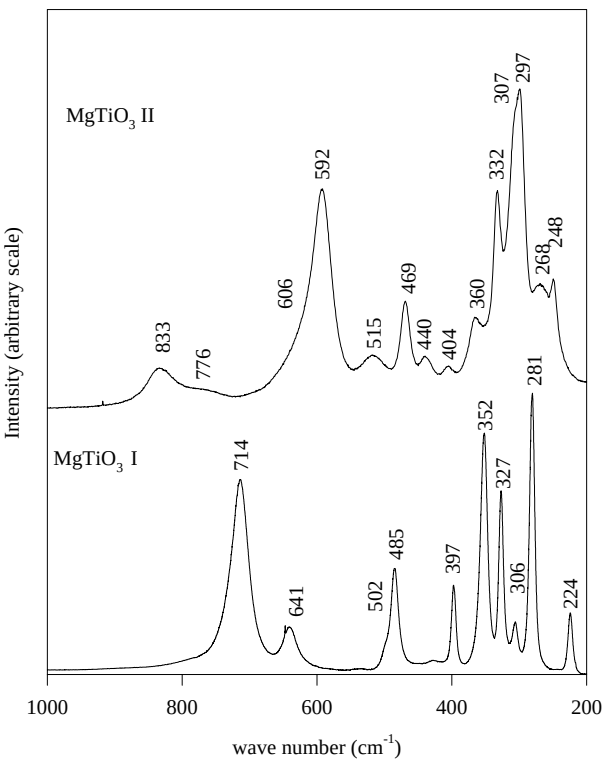

FIGURE 3. Raman spectra of $MgTiO_3$ I and $MgTiO_3$ II, taken from polished crystals at ambient pressure.

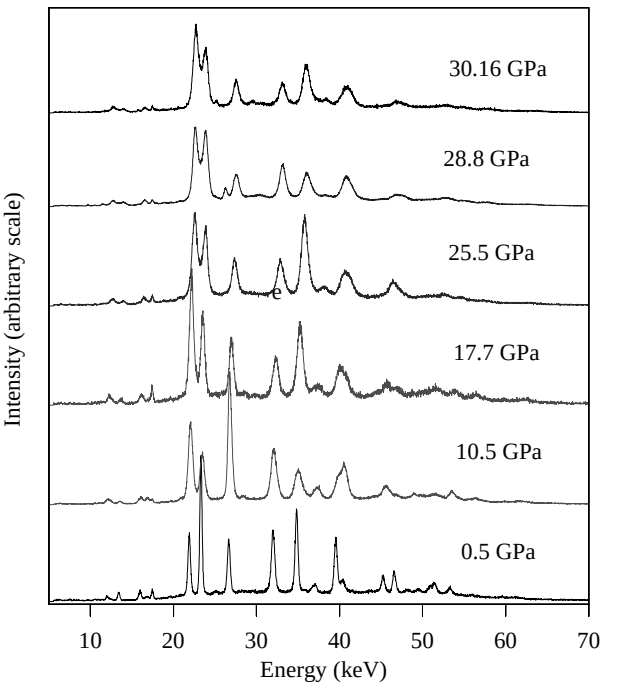

FIGURE 4. Energy-dispersive X-ray diffraction pattern of $(Fe_{0.5}Mg_{0.5})TiO_3$ II as pressure increases during compression in a DAC at room temperature with no pressure medium. At over 28 GPa the region between ~22 and ~24 E/keV can no longer be fit as just two peaks; a new peak is appearing between the original peaks.

volume of the perovskite is 46.43 Å^3 per formula unit at 30 GPa. The most noticeable indication of a phase transition, the appearance of the 112 perovskite peak between the 104 and 110 peaks of the lithium niobate structure, occurs at around 28 GPa at room temperature (Fig. 4).

Upon heating the $Mg_{0.5}Fe_{0.5}TiO_3$ sample to 802 °C, the transformation became more complete and a single phase perovskite was formed (Fig. 5). The volume of the perovskite at 802 °C and 21 GPa is 46.94(11) Å^3 per formula unit (Table 4). After heating, the sample was quenched at pressure from 802 to 300 °C quickly (~30 s), by turning off the small heater inside the cylinder of the DAC, and from 300 °C to room temperature more slowly (greater than one hour for complete cooling) by turning off the large heater external to the cylinder. After complete cooling, the cell was gradually decompressed. During the thermal quenching a two phase mixture of perovskite and ilmenite was formed, the perovskite in this mixture persisted through decompression down to ~8.3 GPa (Fig. 6). Microprobe analysis of the recovered sample from the diamond cell showed segregation into Fe and Mg rich areas. The average compositions were $Mg_{0.622(2)}Fe_{0.418(8)}Ti_{0.980(2)}O_3$ and $Mg_{0.510(20)}Fe_{0.512(20)}Ti_{0.99(10)}O_3$.

Phase diagram

From the thermodynamic data determined through calorimetry (Table 5) and some estimated values of physical parameters (Table 6), the phase relations in the $FeTiO_3$-$MgTiO_3$ system can be calculated. The estimated values are tested by compari-

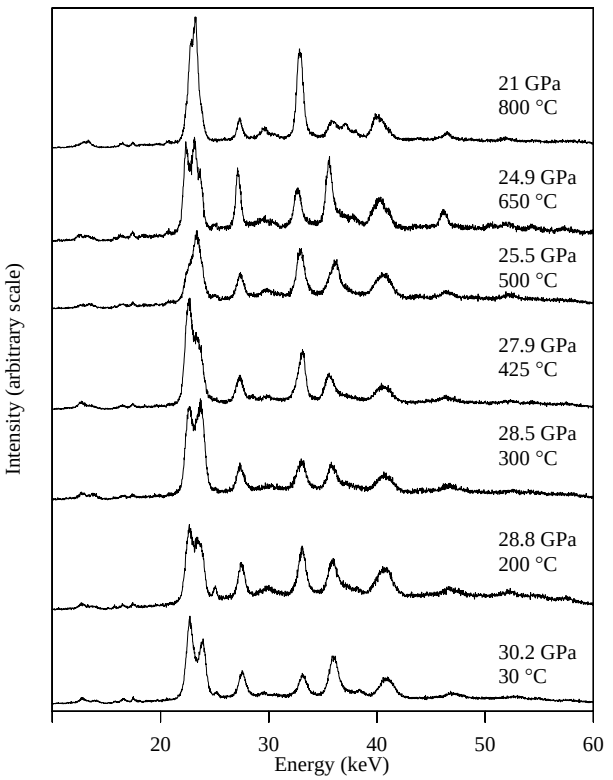

FIGURE 5. Energy-dispersive X-ray diffraction pattern of $(Fe_{0.5}Mg_{0.5})TiO_3$ II as temperature increases and pressure decreases in the diamond cell. Above 21 GPa and 800 °C the $(Fe_{0.5}Mg_{0.5})TiO_3$ II has completely transformed to a $GdFeO_3$-type orthorhombic perovskite [$(Fe_{0.5}Mg_{0.5})TiO_3$ III].

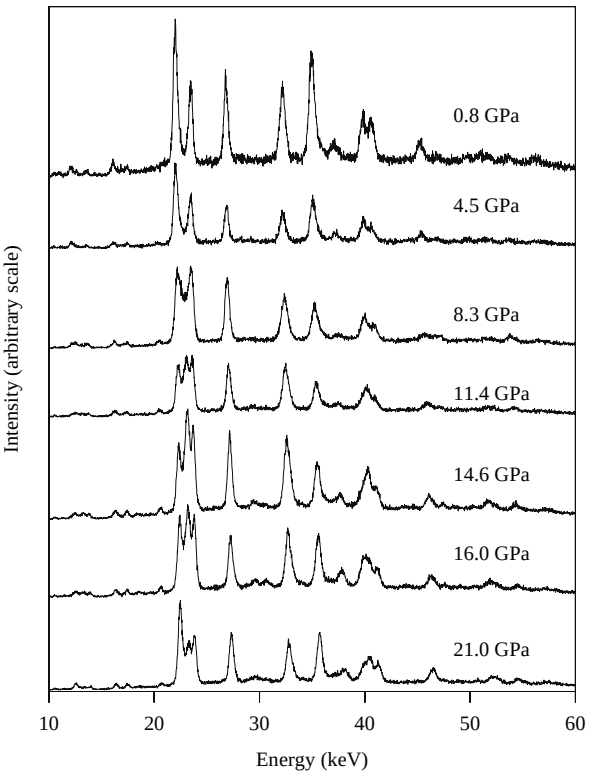

FIGURE 6. Energy-dispersive diffraction spectrum of $(Fe_{0.5}Mg_{0.5})TiO_3$ II as pressure decreases at room temperature in the DAC. Two phases a perovskite and an ilmenite are distinguishable down to ~8.3 GPa.

TABLE 4. X-ray diffraction data for $MgTiO_3$* at 802 °C and 21 GPa

h	*k*	*l*	*d* (obs) (Å)	*d* (calc) (Å)	*d* (diff)	I/I_0
0	0	2	3.611	3.614	–0.003	3
0	2	0	2.608	2.603	0.005	76
1	1	2	2.553	2.551	0.002	92
2	0	0	2.492	2.495	–0.003	6
1	0	3	2.173	2.170	0.003	19
1	1	3	2.007	2.003	0.004	15
1	2	2	1.943	1.945	–0.003	3
0	0	4	1.805	1.807	–0.002	100
1	2	3	1.666	1.667	–0.002	3
1	3	0	1.646	1.640	0.006	12
1	3	1	1.599	1.599	0.001	15
0	3	2	1.560	1.564	–0.004	3
0	2	4	1.486	1.484	0.001	18
2	0	4	1.464	1.463	0.001	3
3	1	2	1.449	1.451	–0.002	8
2	2	4	1.277	1.276	0.001	8
1	1	6	1.143	1.143	0.000	6

Notes: a = 4.9852(69) Å, b = 5.2104(43) Å, c = 7.2305(48) Å, V = 187.75(45) Å^3
* $GdFeO_3$-type perovskite structure.

TABLE 5. Thermochemical data used in phase equilibrium calculations

Transition	ΔH^0_{298} (kJ/mol)	S^0 (J/K-mol)
$FeTiO_3$(I) → $FeTiO_3$(II)	14.5 ± 2.2*	4.9 ± 3.1
$MgTiO_3$(I) → $MgTiO_3$(II)	28.8 ± 1.0†	4.0 ± 2.6
$FeTiO_3$(I) → $FeTiO_3$(III)	27.1 ± 4.0‡	8.9 ± 3.1[c]
$MgTiO_3$(I) → $MgTiO_3$(III)	33.1 ± 5.1§	5.5 ± 2.6[d]
$FeTiO_3$(II) → $FeTiO_3$(III)	12.3 ± 5.9*,‡	4.0 ± 4
$MgTiO_3$(II) → $MgTiO_3$(III)	4.4 ± 6.1†,§	1.5 ± 2

* Calorimetry (Mehta et al. 1994).
† Calorimetry, this study.
‡ High pressure-temperature phase equilibrium, (Syono et al. 1980).
§ High pressure-temperature phase equilibrium, this study.

TABLE 6. Physical properties used in phase equilibrium calculations

Compound	Structure	V^0_{98} (cm^3/mol)		K (GPa)
$MgTiO_3$	ilmenite	30.87*	169#	
$FeTiO_3$	ilmenite	31.70†	177(3)†	
$MgTiO_3$	lithium niobate		30.71‡	172||
$FeTiO_3$	lithium niobate		31.40§	182(7)**
$MgTiO_3$	perovskite	29.31||	225||	
$FeTiO_3$	perovskite	30.15||	236††	

Notes: d*K*/d*P* assumed to be 4. Thermal expansion was assumed equal to that of $FeTiO_3$ ilm, 27.9 × 10^{-6} /K [Wechsler and Prewitt (1984)].
* Wechsler and Von Dreele (1989).
† Wechsler and Prewitt (1984).
‡ Linton et al. (1997).
§ Leinenweber et al. (1995).
|| estimated, see text.
Liebermann (1976).
** Mehta et al. (1994).
†† Leinenweber et al. (1991).

son to the phase stablity data for the end-members.

For the $MgTiO_3$ end-member, thermodynamic data were constrained by the phase stablity and the enthalpy of transition from $MgTiO_3$ I to $MgTiO_3$ II, both from this study. It was first necessary to establish whether the phase boundary, determined through multi-anvil experiments, represented a $MgTiO_3$ I to $MgTiO_3$ II transition or a $MgTiO_3$ I to $MgTiO_3$ III transition

with $MgTiO_3$ II formed metastably during the quench. If we assume that the molar volume change is not a strong function of temperature or pressure for the $MgTiO_3$ I to $MgTiO_3$ II transition [Mehta et al. (1994) showed that ΔV is independent of pressure for $FeTiO_3$], then we can simplify the equation for the free energy of a phase change to:

$$\Delta G(P,T) \approx \Delta H^0 - T\Delta S^0 + P\Delta V^0 \quad (1)$$

At the phase boundary, where $\Delta G = 0$:

$$P \approx \left(\frac{\Delta S}{\Delta V}\right)T - \left(\frac{\Delta H}{\Delta V}\right) \quad (2)$$

For $MgTiO_3$ I $\rightarrow$ $MgTiO_3$ II, $\Delta H_{\text{ilm}\rightarrow\text{lb}} = 28.78 \pm 1.45$ kJ/mol (this study), $\Delta V^0_{\text{lm}\rightarrow\text{lb}} = -0.16$ cm^3/mol (Linton et al. 1997), and we calculate the $T = 0$ K intercept of the transition to be $(\Delta H/\Delta V) = 179 \pm 1$ GPa. This value can be compared to the $T = 0$ K intercept from the equation of the phase boundary obtained in this study: P(GPa) = –0.008(2)T(K) + 33(4) (GPa). Clearly the 179 ± 1 GPa calculated is much higher than the 33 ± 4 GPa observed, and the phase boundary from multi-anvil experiments is not the $MgTiO_3$ I to $MgTiO_3$ II boundary; rather, analogously to $FeTiO_3$ (Mehta et al. 1994), it is most likely the $MgTiO_3$ I to $MgTiO_3$ III boundary with $MgTiO_3$ II as a quench product.

The phase diagram of the $FeTiO_3$-$MgTiO_3$ join at pressure can be calculated by simultaneously solving the following equations;

$$\Delta H^0_{\text{MgTiO}_3}(\text{il}\rightarrow\text{pv}) - T\Delta S^0_{\text{MgTiO}_3}(\text{il}\rightarrow\text{pv}) + \int_{1\text{atm}}^{P}\Delta V^0_{\text{MgTiO}_3}(\text{il}\rightarrow\text{pv})\text{d}P + \text{R}T\ln\left(\frac{a^{\text{pv}}_{\text{MgTiO}_3}}{a^{\text{il}}_{\text{MgTiO}_3}}\right) = 0 \quad (3)$$

$$\Delta H^0_{\text{FeTiO}_3}(\text{il}\rightarrow\text{pv}) - T\Delta S^0_{\text{FeTiO}_3}(\text{il}\rightarrow\text{pv}) + \int_{1\text{atm}}^{P}\Delta V^0_{\text{FeTiO}_3}(\text{il}\rightarrow\text{pv})\text{d}P + \text{R}T\ln\left(\frac{a^{\text{pv}}_{\text{FeTiO}_3}}{a^{\text{il}}_{\text{FeTiO}_3}}\right) = 0 \quad (4)$$

where S is entropy and a is activity. We model the activity by assuming the ideal case $\gamma = 1$, where the activity, a_j, simply equals the mole fraction, X_j, or another approach employs nonideal mixing models. The $MgTiO_3$-$FeTiO_3$ join for the ilmenite structure has been described by a symmetrical regular mixing model, $\text{R}T\ln\gamma_j = W_G(1-X\alpha_j)^2$, where $W_G = 4300$ J/mol, based on partitioning of Mg and Fe between coexisting ilmenites and olivines (Andersen et al. 1991). Using the method of Davies and Navrotsky (1983), which correlates the interaction parameter with the volume mismatch of the two end-members, we estimated symmetric W_G values as 2278 J/mol, 2163 J/mol, and 1824 J/mol, respectively, for Mg-Fe mixing in the ilmenite, perovskite, and lithium niobate structures. With these nonideal mixing models, Equations 3 and 4 become:

$$\Delta H^0_{\text{MgTiO}_3}(\text{il}\rightarrow\text{pv}) - T\Delta S^0_{\text{MgTiO}_3}(\text{il}\rightarrow\text{pv}) + \int_{1\text{atm}}^{P}\Delta V^0_{\text{MgTiO}_3}(\text{il}\rightarrow\text{pv})\text{d}P + \text{R}T\ln\left(\frac{X^{\text{pv}}_{\text{MgTiO}_3}}{X^{\text{il}}_{\text{MgTiO}_3}}\right) - W_G\left(X^{\text{il}}_{\text{FeTiO}_3}\right)^2 + W_{G_{\text{pv}}}\left(X^{\text{pv}}_{\text{FeTiO}_3}\right)^2 = 0 \quad (5)$$

and:

$$\Delta H^0_{\text{FeTiO}_3}(\text{il}\rightarrow\text{pv}) - T\Delta S^0_{\text{FeTiO}_3}(\text{il}\rightarrow\text{pv}) + \int_{1\text{atm}}^{P}\Delta V^0_{\text{FeTiO}_3}(\text{il}\rightarrow\text{pv})\text{d}P + \text{R}T\ln\left(\frac{X^{\text{pv}}_{\text{FeTiO}_3}}{X^{\text{il}}_{\text{FeTiO}_3}}\right) - W_G\left(X^{\text{il}}_{\text{MgTiO}_3}\right)^2 + W_{G_{\text{pv}}}\left(X^{\text{pvl}}_{\text{MgTiO}_3}\right)^2 = 0 \quad (6)$$

These two equations were solved for different values of W_G(il) and W_G(pv) using Newton's method, with starting values for composition from the exact solutions of Equation 3 assuming ideal mixing, to obtain the phase diagram at 802 °C (Fig. 7). Ideal mixing best predicts the compositions of the two phases in the recovered sample from the DAC, although that experiment does not necessarily define an equilibrium pair of compositions at any P and T.

DISCUSSION

Petrological implications

The high-pressure phase diagram of the $FeTiO_3$-$MgTiO_3$ join can be applied to ultra-high pressure metamorphic rocks and kimberlites. Dobrzhinetskaya et al. (1996) found ilmenite inclu-

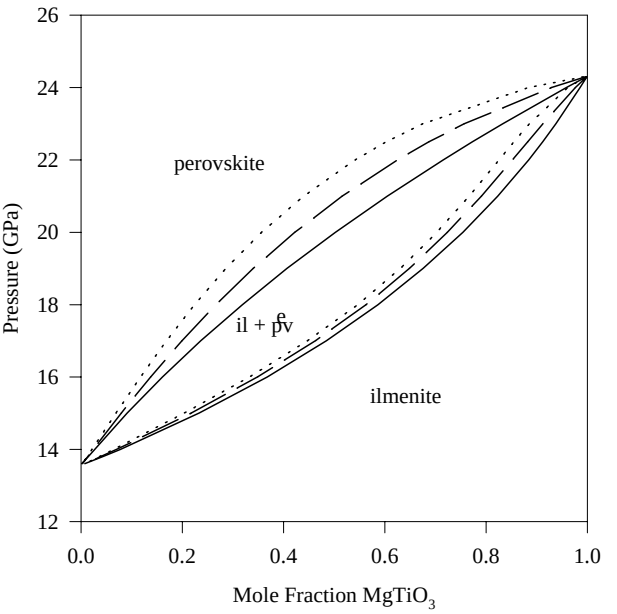

FIGURE 7. Calculated phase diagram for the $FeTiO_3$-$MgTiO_3$ join at 800 °C. The two phase loops for the ilmenite to perovskite transition were calculated using W_G(il) = 4300 J/mol and W_G(pv) = 4300 J/mol (dotted curve), W_G(il) = 2278 J/mol and W_G(pv) = 2163 J/mol (dashed curve). The solid curve represents ideal mixing.

sions with unique structures in olivine from ultra-high-pressure rocks from the Alpe Arami peridotite; garnet-orthopyroxene-clinopyroxene equilibration in these rocks indicates pressures from 4 to 5 GPa and temperatures from 900 to 1000 °C. However, the volume of exsolved chromite and $FeTiO_3$ in olivines was greater than could be explained by any documented substitution of Cr^{3+} and Ti^{3+} into the olivine structure, and Dobrzhinetskaya et al. (1996) postulated that the inclusions reflect an even higher pressure precursor phase, such as $(Mg_{0.9}Fe_{0.1})_2SiO_4$ in the β-phase, which accommodates a higher substitution of trivalent cations. This implies that these rocks reached pressures above 14 GPa, high enough to stabilize iron-rich (Fe,Mg)TiO_3 III . The topotaxially oriented (Fe,Mg)TiO_3 rod-shaped precipitates in olivine have orthorhombic crystal structures with lattice parameters: a = 0.470 nm, b = 1.028 nm, c = 0.574 nm. Dobrzhinetskaya et al. (1996) propose that during uplift β-phase transformed to olivine from which crystallographically oriented (Fe,Mg)TiO_3 III exsolved [(Fe,Mg)TiO_3 I exsolves from olivine with no preferred orientation]. The observed orthorhombic crystals would then be metastable decomposition structures from (Fe,Mg)TiO_3 III.

(Fe,Mg)TiO_3 II was not observed, possibly due to topotaxial constraints and/or slower cooling rates which might avoid this metastable phase. For the set of reactions to occur as Dobrzhinetskaya et al. (1996) propose, the transformation from β-phase to olivine must occur before the transformation of (Fe,Mg)TiO_3 III to ilmenite (I). Using the phase boundary of Syono et al. (1980) for pure $FeTiO_3$, this is a certainty, but from our study it becomes plain that which transformation occurs first during uplift is very much a function of the $MgTiO_3$ content of the (Fe,Mg)TiO_3 III, which Dobrzhinetskaya et al. (1996) were not able to accurately determine. Whether or not the (Fe,Mg)TiO_3 structures of the Alpe Arami are remnants of the (Fe,Mg)TiO_3 III phase, they are a good example of the petrological importance of the high *P* and *T* phase relations of the $FeTiO_3$-$MgTiO_3$ join.

Two other (Fe,Mg)TiO_3 phases exist in the natural olivines that Dobrzhinetskaya et al. (1996) conjecture are intermediates between the orthorhombic (Fe,Mg)TiO_3 and (Fe,Mg)TiO_3 I. One of these intermediates has reported lattice parameters of $a \cong 0.470$ nm, $b \cong 0.5014$ nm, $c \cong 0.574$ nm. This phase has an even smaller unit cell volume than the $Mg_{0.5}Fe_{0.5}TiO_3$ III observed in our DAC studies. The persistence of perovskite during the slow cooling of the diamond cell from 300 °C to room temperature indicates that at low temperatures perovskite may persist metastably to pressures below the ilmenite-perovskite transition. If the olivine were exerting a confining pressure on the (Fe,Mg)TiO_3 phase, it might be worthwhile to reexamine the TEM data of Dobrzhinetskaya et al. (1996) keeping in mind the possibility of metastable perovskite structures.

Systematics of ilmenite-lithium niobate-perovskite phase transitions

Previous X-ray diffraction of $MnTiO_3$ and $FeTiO_3$ in a DAC showed that the lithuim niobate structure (II) phase transformed to a perovskite (III) at high pressure, but some uncertainty remained as to which structure was stable at high temperature and high pressure (Ross et al. 1989; Leinenweber et al. 1991). Whereas Mehta et al. (1994) concluded $FeTiO_3$ III was the stable phase at high pressure and temperature, Ko et al. (1989) suggested that $MnTiO_3$ II, which was stable under high-temperature and high-pressure conditions and that $MnTiO_3$ III was only stable under high-pressure, low-temperature conditions. Here, $Fe_{0.5}Mg_{0.5}TiO_3$ sample show, $Fe_{0.5}Mg_{0.5}TiO_3$ III is the stable phase at high temperature and high pressure. Reexamining the $MnTiO_3$ data with the assumption, based our observations of the $FeTiO_3$-$MgTiO_3$ join, that the I to III transition must have a positive ΔS leads us to the conclusion that $MnTiO_3$ III is also the stable high-temperature and high-pressure phase in this system. Our new understanding of the energetics of I-II-III transitions in $FeTiO_3$-$MgTiO_3$ may also allow predictions to be made for other titanates.

Figure 8 shows the relationship between "A" cation size and the energetic barrier to forming a perovskite. The "A" cation radius of Ca is 1.00 Å, and $CaTiO_3$ is stable as a perovskite at room temperature and pressure. $BaTiO_3$ has "A" cation radii greater than 1 Å, is stable at room temperature and pressure as a perovskite, and has a high temperature hexagonal polymorph (not an ilmenite structure). The ΔH^0_{298}(hex → pv) of this transition does not fall on the line for ilmenite-perovskite transitions.

The ΔH^0 of transition between II and I increases linearly with Mg content (Fig. 9). Similarly, $\Delta H^0_{I \rightarrow II}$ can be shown to be a linear function of "A" cation radius (in sixfold coordination). This relationship holds even when other titanates, such as $MnTiO_3$ (Ko et al. 1989), are included. The titanate "A" cation radius also depends linearly on the 0 K pressure of transition from ilmenite to perovskite (Fig. 10), except that $CdTiO_3$,with an "A" cation radius of 0.95 Å, falls off the trend at negative ΔH^0. $CdTiO_3$ is the only one of the four titanates

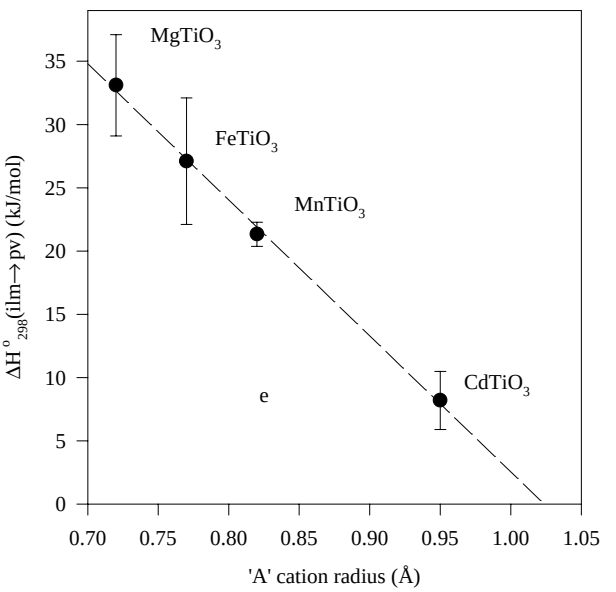

FIGURE 8. ΔH_{98}(ilm→ pv) vs. the "A" cation ionic radius in sixfold coordination of the titanates from this study, plus $CdTiO_3$ (Takayama-Muromachi and Navrotsky 1988) and $MnTiO_3$ (Ko et al. 1989). The line is a best fit with a ΔH_{98} = 0 intercept of 1.02 ± 0.04 Å.

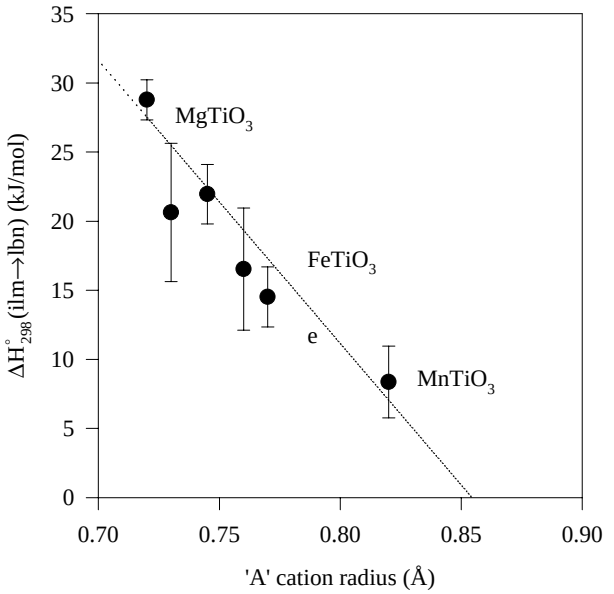

FIGURE 9. ΔH_{98}(ilm→ lbn) vs. the "A" cation ionic radius in sixfold coordination of the titanates from this study, plus $MnTiO_3$ (Ko et al. 1989). Line is best fit line with a $\Delta H^0_{298} = 0$ intercept of 0.85 ± 0.05 Å.

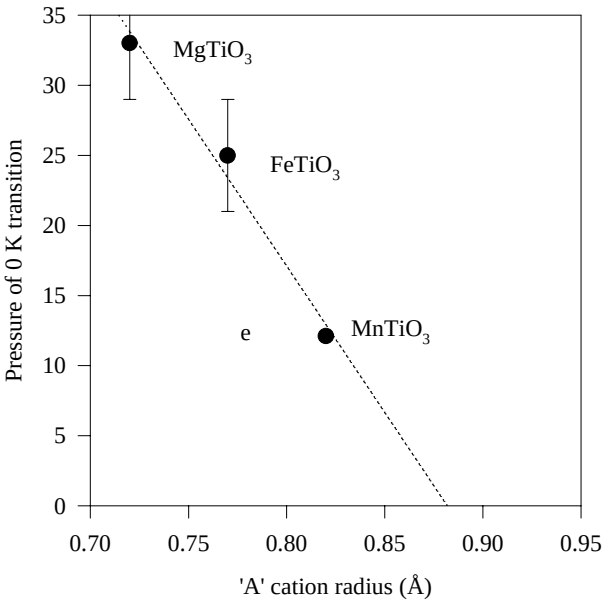

FIGURE 10. The "A" cation ionic radius in sixfold coordination vs. the 0 K pressure of transition from ilmenite to perovskite from phase equilibria studies: $MgTiO_3$ from this study, $FeTiO_3$ from Syono et al. (1980), $MnTiO_3$ from Ko et al. (1989). The dotted line is a best fit with a $P = 0$ intercept at 0.88 ± 0.04 Å.

($CdTiO_3$, $FeTiO_3$, $MgTiO_3$, and $MnTiO_3$) which can be synthesized at atmospheric pressure in the perovskite structure, and $CdTiO_3$, unlike $FeTiO_3$, $MgTiO_3$, and $MnTiO_3$, does not have a lithium niobate quench phase.

The similar intercepts for the ΔH^0_{298}(ilm → lb) and 0 K pressure of transition plots (Figs. 8–10) suggest that for titanates the upper limit of "A" cation radius for compounds with a lithium niobate quench phase is ~0.86 ± 0.15. We can predict on this basis that $NiTiO_3$ (Ni ionic radius = 0.70) and $CoTiO_3$ (Co ionic radius = 0.735) will have high-pressure perovskite polymorphs that will quench to lithium niobate structures on release of pressure. This correlation, if it holds for minerals other than titanates, could be used as a useful indicator of the stability of lithium niobate type minerals. This result also indicates that Fe is not acting differently from Mg due to its electronic structure, as had previously been suggested by Reynard and Guyot (1994); the size of the "A" cation governs stability.

Different $A^{2+}B^{3+}O_3$ oxides with perovskite structure types are compared using a Goldschmidt diagram, Figure 11 (Ringwood 1970). Because this type of diagram is typically used to designate fields for structures such as garnet, pyroxene, and ilmenite where the "A" and "B" cations are in sixfold coordination, the "A" and "B" cation ionic radii (r_A and r_B) plotted are with a sixfold coordination with values taken from Shannon and Prewitt (1969). The tolerance factors:

$$t = (r_A + r_O) / [2(r_B + r_O)]^{1/2}$$

shown are a measure of the size mismatch for sixfold coordination. Tolerance factors are approximately five (more or less, depending on the A cation) less than the Goldschmidt tolerance factors for perovskites, which are calculated with the "A"

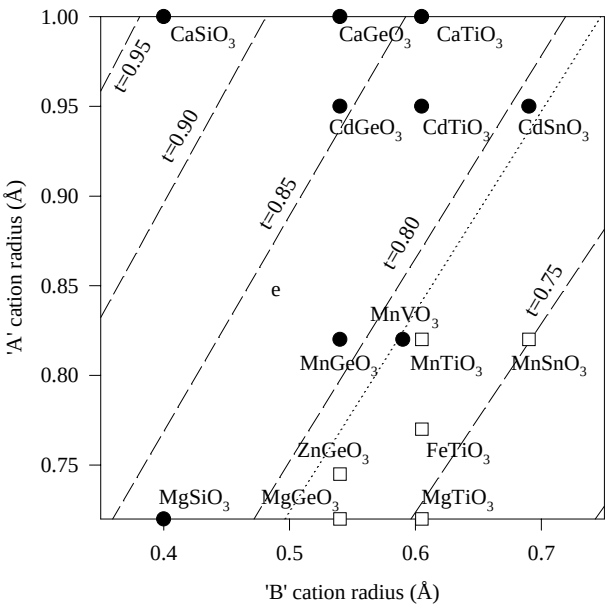

FIGURE 11. Goldschmidt diagram, based on Leinenweber et al. (1991), plots the "B" cation radius in sixfold coordination vs. the "A" cation radius also in sixfold coordination of selected ABO_3 compounds. Filled circles are perovskite forming compounds with no lithium niobate quench phase. Open squares have lithium niobate quench structure. Dashed lines are tolerance factors. Dotted line is the our calculated upper tolerance limit for compounds to have lithium niobate quench structure (see text).

cation in eightfold coordination, as it would be in perovskite. The ideal cubic perovskite structure would have a Goldschmidt tolerance factor equal to one. However, for ilmenites and lithium niobates, where the "A" cation is in sixfold coordination, plotting a tolerance factor based on the "A" cation radii from sixfold coordination is more convenient. The upper limit for "A" cation radius for a titanate which will form a lithium niobate quench product corresponds to a tolerance factor of 0.79 ± 0.01 Å (with "A" in an sixfold coordination). This value agrees well with the behavior of other ABO_3 compounds plotted (Fig. 11).

These results can also be compared to the arguments in Funamori et al. (1997) for the existence of a $LiNbO_3$ quench phase of natural garnet with a composition between $Mg_4Si_4O_{12}$ and $Mg_3Al_2Si_3O_{12}$. Funamori et al. (1997) calculate tolerance factors for $Mg_4Si_4O_{12}$ and $Mg_3Al_2Si_3O_{12}$ using "A" cations in sixfold coordination. They claim the *t* values they calculate, 0.83 and 0.80 respectively, are below the expected *t* values, $t > 0.85$, for samples quenching to rhombohedral perovskites, but they are just above our limit for lithium niobate quench products. A sample with a composition between $Mg_4Si_4O_{12}$ and $Mg_3Al_2Si_3O_{12}$ might have too high a tolerance to yield a lithium niobate quench product; however, as they predict, with increasing Al content the likelihood of quenching to lithium niobate would increase.

ACKNOWLEDGMENTS

This work was supported by the Center for High Pressure Research, a NSF Science and Technology Center.

REFERENCES CITED

Andersen, D.J., Bishop, F.C., and Lindsley, D.H. (1991) Internally consistent solution models for Fe-Mg-Mn-Ti oxides: Fe-Mg-Ti oxides and olivine. American Mineralogist, 76, 427–444.

Anderson, O.L., Isaak, D.G., and Yamato, S. (1989) Anharmonicity and the equation of state for gold. Journal of Applied Physics, 65, 1534–1543.

Bertka, C.M. and Fei, Y. (1996) Constraints on the mineralogy of an iron-rich Martian mantle from high-pressure experiments. Planetary and Space Science, 44, 1269–1276.

Brown, N.E. and Navrotsky, A. (1994) Hematite-ilmenite (Fe_2O_3-$FeTiO_3$) solid solutions: The effects of cation ordering on the thermodynamics of mixing. American Mineralogist, 79, 485–496.

Dobrzhinetskaya, L., Green, H.W., and Wang, S. (1996) Alpe Arami: A peridotite massif from depths of more than 300 kilometers. Science, 271, 1841–1845.

Fei, Y. (1996) Crystal chemistry of FeO at high pressure and temperature. In Dyar M.D. McCammon, C.A., and Schaefer Eds., Mineral Spectroscopy: A tribute to Roger G. Burns. Special publication No. 5, Geochemical Society, Houston, TX, pp 234–254.

Funamori, N., Yagi, T., Miyajima, N., and Fujino, K. (1997) Transformation in garnet from orthorhombic perovskite to $LiNbO_3$ phase on release of pressure. Science, 275, 513–515.

Ghiorso, M.S. (1990) Thermodynamic properties of hematite-ilmenite-geikielite solid solutions. Contributions Mineralogy and Petrology 104, 645–667.

Knittle, E. (1995) Static compression measurements of equations of state. In Ahrens, T. Ed. Mineral Physics and Crystallography: A handbook of physical constants. AGU reference shelf 2, American Geophysical Union, Washington, D.C.

Ko, J. and Prewitt, C.T. (1988) High-pressure phase transition in $MnTiO_3$ from the ilmenite to the $LiNbO_3$ structure. Physics and Chemistry of Minerals, 15, 355–362.

Ko, J., Brown, N.E., Navrotsky, A., Prewitt, C.T., and Gasparik, T. (1989) Phase equilibrium and calorimetric study of the transition of $MnTiO_3$ from the ilmenite to the lithium niobate structure and implications for the stability field of perovskite. Physics and Chemistry of Minerals, 16, 727–733.

Leinenweber, K., Utsumi, W., Tsuchida, Y., Yagi, T., and Kurita, K. (1991) Unquenchable high-pressure perovskite polymorphs of $MnSnO_3$ and $FeTiO_3$. Physics and Chemistry of Minerals 18, 244–250.

Leinenweber, K., Linton, J., Navrotsky, A., Fei, Y., and Parise, J.B. (1995) High-pressure perovskites on the join $CaTiO_3$-$FeTiO_3$. Physics and Chemistry of Minerals, 22, 251–258.

Liebermann, R.C. (1976) Elasticity of ilmenites. Physics of Earth and Planetary Interiors, 12, 5–10.

Linton, J.A., Fei, Y., and Navrotsky, A. (1997) Complete Fe-Mg solid solution in lithium niobate and perovskite structures in titanates at high pressures and temperatures. American Mineralogist, 82, 639–642.

Mehta, A., Leinenweber, K., and Navrotsky, A. (1994) Calorimetric study of high pressure polymorphism in $FeTiO_3$: The stability of the perovskite phase. Physics and Chemistry of Minerals, 21, 207–212.

Navrotsky, A. (1997) Progress and new directions in high temperature calorimetry revisited. Physics and Chemistry of Minerals, 24, 222–241.

Reynard, B. and Guyot, F. (1994) High-temperature properties of geikielite ($MgTiO_3$-ilmenite) from high temperature high-pressure Raman spectroscopy—some implications for $MgSiO_3$-ilmenite. Physics and Chemistry of Minerals, 21, 441–450.

Ringwood, A.E. (1970) Phase transformations and the constitution of the mantle. Physics of the Earth and Planetary Interiors, 3, 109–155.

Robie, R.A. and Hemingway, B.S. (1995) Thermodynamic properties of minerals and related substances at 298.15 K and 1 bar (10^5 Pascals) pressure and at higher temperatures. U.S. Geological Survey Bulletin, 2131.

Robie, R.A., Hemingway, B.S., and Fisher, J.R. (1978) Thermodynamic properties of minerals and related substances at 298.15 K and 1 bar (10^5 Pascals) pressure and at higher temperatures. U.S. Geological Survey Bulletin, 1452.

Ross, N.L., Ko, J., and Prewitt, C.T. (1989) A new phase transition in $MnTiO_3$: $LiNbO_3$-perovskite structure. Physics and Chemistry of Minerals, 16, 621–629.

Shannon, R.D. and Prewitt, C.T. (1969) Effective ionic radii in oxides and fluorides. Acta Crystallographica, B25, 925–946.

Syono, Y., Yamauchi, H., Ito, A., Someya, Y., Ito, E., Matsui, Y., Akaogi, M., and Akimoto, S. (1980) Magnetic properties of the disordered ilmenite $FeTiO_3$ II synthesized at very high pressure. In H. Watanabe, S. Iida, and Y. Sugimoto, Eds., Ferrites: Proceedings of the International Conference, p. 192–195. Tokyo, Japan.

Takayama-Muromachi, E. and Navrotsky, A. (1988) Energetics of compounds ($A^{2+}B^{3+}O_3$) with the perovskite structure. Journal of Solid State Chemistry, 72, 244–256.

Topor, L. and Navrotsky, A. (1992) Advances in calorimetric techniques for high pressure phases. In Y. Syono and M. Manghnani, Eds. High pressure research: Application to earth and planetary sciences, p. 71–76. Terra Publishing Co., Tokyo, Japan and American Geophysical Union, Washington, D.C.

Wechsler, B.A. and Navrotsky, A. (1984) Thermodynamics and structural chemistry of compounds in the system MgO-TiO_2. Journal of Solid State Chemistry, 55, 165–180.

Wechsler, B.A. and Prewitt, C.T. (1984) Crystal structure of ilmenite ($FeTiO_3$) at high temperature and at high pressure. American Mineralogist, 69, 176–185.

Wechsler, B. and Von Dreele, R.B. (1989) Structure refinements of Mg_2TiO_4, $MgTiO_3$ and $MgTi_2O_5$ by time-of-flight neutron powder diffraction. Acta Crystallographica, B45, 542–549.

Wood, B.J., Nell, J., and Woodland, A.B. (1991) Macroscopic and microscopic thermodynamic properties of oxides. In Mineralogical Society of America Reviews in Mineralogy, 25, 265–299.

MANUSCRIPT RECEIVED FEBRUARY 17, 1998
MANUSCRIPT ACCEPTED JUNE 4, 1999
PAPER HANDLED BY ANASTASIA CHOPELAS